DTIC FILE COPY

JMENTATION PAGE

Form Approved
OMB No. 0704-0188

is estimated to average 1 hour per response, including the time for reviewing instructions, searching existing data sources, gathering and reviewing the collection of information. Send comments regarding this burden estimate or any other aspect of reducing this burden, to Washington Headquarters Services, Directorate for Information Operations and Reports, 1215 Jefferson and to the Office of Management and Budget, Paperwork Reduction Project (0704-0188), Washington, DC 20503.

AD-A223 655

Report Date.	3. Report Type and Dates Covered.
May 15, 1990	Journal Article

4. Title and Subtitle.
A Comparison Between the Generalized Digital Environmental Model and Levitus Climatologies

5. Funding Numbers.
Program Element No. 62435N
Project No. 3584
Task No. 803
Accession No. DN256002

6. Author(s).
Teague, W. J., M.J. Carron, & P. J. Hogan

7. Performing Organization Name(s) and Address(es).
Naval Oceanographic and Atmospheric Research Laboratory
Ocean Science Directorate
Stennis Space Center, MS

8. Performing Organization Report Number.
JA 331:057:89

9. Sponsoring/Monitoring Agency Name(s) and Address(es).
Naval Oceanographic and Atmospheric Research Laboratory
Ocean Science Directorate
Stennis Space Center, MS

10. Sponsoring/Monitoring Agency Report Number.
JA 331:057:89

11. Supplementary Notes.
Naval Oceanographic Office (1)
Stennis Space Center, MS

Sverdrup Technology, Incorporated (2)
Stennis Space Center, MS

12a. Distribution/Availability Statement.
Approved for public release; distribution is unlimited

12b. Distribution Code

DTIC ELECTE JUN 29 1990 S C B D

13. Abstract *(Maximum 200 words).*

Two ocean climatologies of temperature and salinity, the Generalized Digital Environmental Model (GDEM) and the Climatological Atlas of the World Ocean, are compared. Dynamic height fields are computed by season from each climatology for the North Atlantic, North Pacific, and Indian oceans and are compared on a 1 degree latitude-longitude grid. Large-scale oceanographic features are generally found to be similarly represented in both climatologies. GDEM appears to render better representations of seasonal variability and regions of high current shear, such as the Gulf Stream, because of a different smoothing method and a finer grid spacing. Maps of dynamic heights from both climatologies are presented, and their similarities and differences are discussed. The methodology for the construction of GDEM is also described in detail.

14. Subject Terms.
Data base, climatology, mesoscale oceanography, GDEM

15. Number of Pages.
17

16. Price Code.

17. Security Classification of Report.	18. Security Classification of This Page.	19. Security Classification of Abstract.	20. Limitation of Abstract.
Unclassified	Unclassified	Unclassified	SAR

JOURNAL OF GEOPHYSICAL RESEARCH, VOL. 95, NO. C5, PAGES 7167–7183, MAY 15, 1990

A Comparison Between the Generalized Digital Environmental Model and Levitus Climatologies

WILLIAM J. TEAGUE

Naval Ocean Research and Development Activity, Stennis Space Center, Mississippi

MICHAEL J. CARRON

Naval Oceanographic Office, Stennis Space Center, Mississippi

PATRICK J. HOGAN

Sverdrup Technology, Incorporated, Stennis Space Center, Mississippi

Two ocean climatologies of temperature and salinity, the Generalized Digital Environmental Model (GDEM) and the Climatological Atlas of the World Ocean, are compared. Dynamic height fields are computed by season from each climatology for the North Atlantic, North Pacific, and Indian oceans and are compared on a 1° latitude-longitude grid. Large-scale oceanographic features are generally found to be similarly represented in both climatologies. GDEM appears to render better representations of seasonal variability and regions of high current shear, such as the Gulf Stream, because of a different smoothing method and a finer grid spacing. Maps of dynamic heights from both climatologies are presented, and their similarities and differences are discussed. The methodology for the co. struction of GDEM is also described in detail.

1. INTRODUCTION

Ease of access to data that have been taken in situ is essential for improving our understanding of ocean dynamics. Data have been accumulating for more than 100 years, and the last 40 years have produced both temperature and salinity measurements extensive and accurate enough to use in estimates of the global density fields. These data, which are normally stored in data bases, also reside in condensed, analyzed form as climatologies. A comparison of two of the better known climatologies is the subject of this paper.

Climatologies consist of data averaged over well-defined spatial grids and over time periods such as months, seasons, or years. A broad distribution of the data in time and in space is best for the formulation of representative profiles in the construction of climatologies. Data-scarce situations require special averaging and interpolation techniques to get acceptable results. Accurate climatologies on basin scales are particularly important for numerical model development and evaluation, for quality control of other data sets, for climate studies, and for the design of experiments. One of the most useful products derived from climatologies is the representation of data fields in an atlas format on seasonal time scales.

Oceanographic atlases, consisting of specific data fields on map bases, are the predecessors to climatologies. An outstanding early atlas is the Meteor Atlas [*Wüst and Defant*, 1936]. Other important past atlases include the Robinson-Bauer atlases [*Robinson et al.*, 1979; *Robinson*, 1976], Fuglister's atlas of the Atlantic Ocean [*Fuglister*, 1960], Worthington's North Atlantic atlas [*Worthington and Wright*, 1970], and Wyrtki's atlas of the Indian Ocean [*Wyrtki*, 1971]. A catalogue of oceanographic atlases prepared by *Stommel and Fieux* [1978] shows no data sets in the form of global climatologies before the two being compared here.

Levitus [1982] published the first worldwide climatology, The Climatological Atlas of the World Ocean (hereafter referred to as LC), basing it on objectively analyzed, gridded sets of temperature, salinity, and oxygen fields. LC provides a synthesis of all temperature, salinity and oxygen data that were available from the National Oceanographic Data Center (NODC), Washington, D. C., through 1977. The data were analyzed on annual, seasonal, and monthly time scales and were gridded in 1° latitude-longitude cells at standard oceanographic levels between the ocean surface and bottom (maximum depth 5500 m).

The other climatology being considered here, the Generalized Digital Environmental Model (GDEM) [*Davis et al.*, 1986] had its beginnings at the Naval Oceanographic Office (NAVOCEANO) in 1975. GDEM is a four-dimensional (latitude, longitude, depth, and time) digital model of temperature and salinity for the North and South Atlantic, and Pacific north of the equator, the Indian Ocean north of 40°S, the Arctic Ocean, the Mediterranean Sea, and the Black Sea. The South Pacific model is expected to be finished by October 1989. GDEM consists of coefficients of mathematical expressions describing vertical profiles of temperature and salinity on a $\frac{1}{2}$° latitude-longitude grid for seasonal and annual time frames. Profiles of temperature and salinity are generated from equations using the stored coefficients. Data for building the current version of GDEM were obtained from the 1986 version of the Master Oceanographic Observational Data Set (MOODS) [*Bauer*, 1985; *Teague et al.*, 1987], supplemented by other data holdings at NAVOCEANO. The South Atlantic and South Pacific models in GDEM, however, rely heavily on LC.

This paper is not subject to U.S. copyright. Published in 1990 by the American Geophysical Union.

Paper number 89JC03682.

90 06 27 077

GDEM is used by the U.S. Navy for most of its operational systems. By contrast, LC is generally used by both the academic community and the Navy (particularly when global coverage is required). The reasons for these preferences are not clear, aside from the question of accessibility. No comparison between the two climatologies has hitherto been made. In this paper we amend that situation by comparing dynamic heights computed over ocean basins from GDEM and LC on seasonal and annual scales. We discuss the similarities between the data sets and the differences.

In section 2 we describe GDEM for the first time in the open literature and discuss the plans for development of future GDEMs. The method used in building the LC is presented in section 3. Intercomparison methods are discussed in section 4, and section 5 describes seasonal anomalies within GDEM and within LC. Differences between GDEM and LC are presented in section 6, and the results are discussed and summarized in section 7.

2. GDEM Description

GDEM has been constructed over the last 14 years through the efforts of many NAVOCEANO personnel. The current master GDEM [*Davis et al.*, 1986] is formed from about 4 million temperature and salinity profiles, primarily from the MOODS. Quality control of these data has included examining range and static stability, checking for data that are misplaced either by location or by season, and checking for duplicate profiles. GDEM consists of sets of coefficients for temperature and salinity, gridded at 30 arc-minutes in space, and in 3-, 6-, or 12-month time frames. The exception to these quantizations are the coefficients describing sea surface temperature, which are gridded at 1-month intervals. Utilizing these coefficient sets with the appropriate one-dimensional functional forms, and with one-dimensional linear or cubic spline interpolation in time, vertical profiles of historical temperature and salinity extending from the surface to the bottom may be computed for any desired point in time for all water depths greater than 100 m. High-resolution GDEMs have been built for selected areas on 10′ × 10′ or finer grids. Additionally, three regions (Gulf Stream, Kuroshio/Oyashio, and Iceland-Faeroe Gap) are modeled by versions called the "Dynamic GDEMs," which have the capability of allowing fronts and rings to be represented very shortly after appropriate in situ data have been taken.

The basic design concept of GDEM is the determination of a set of analytical curves that represent the mean vertical distributions of temperature and salinity for grid squares through the averaging of the coefficients of the mathematical expressions for the curves found for individual profiles. The averaged coefficients for data sets can be shown to be not the same as coefficients of averaged data. Different families of representative curves have been chosen for shallow, mid-depth, and deep ranges, with each chosen so that the number of parameters required to yield a smooth, mean profile over the range was minimized. The matching conditions through the depth range transitions are chosen so that no discontinuities in vertical gradients occur. During the GDEM modeling procedure, temperature and salinity determinations are processed independently. This allows the results to be checked for stable densities and serves as a means for utilizing observations from vast numbers of expendable bathythermographs. The various separate submodels and functional forms which compose the current GDEM are summarized in Table 1.

TABLE 1. The Generalized Digital Environmental Model: Type and Form of Submodels

	Submodel Form
Shallow Top Submodel	
Temperature	
0–400 m (20-m levels)	eight coefficients, nonlinear
3-month seasons	least squares
1-month sea surface	rms error of fit <0.5°C
Salinity	
0–400 m (20-m levels)	five-degree orthogonal polynomial
5-month seasons	rms error of fit <0.1‰
Middepth Submodel	
Temperature	
200–2450 m (50-m levels)	seven-degree orthogonal polynomial
6-month seasons	rms error of fit <0.25°C
Salinity	
200–2450 m (50-m levels)	five-degree orthogonal polynomial
6-month Seasons	rms error of fit <0.05‰
Deep Submodel	
Temperature	
2000-m bottom (standard levels)*	quadratic
12-month seasons	rms error of fit <0.25°C
Salinity	
2000-m bottom (standard levels)*	quadratic
12-month seasons	rms error of fit <0.05‰

*Standard levels: 0, 10, 20, 30, 50, 75, 100, 125, 150, 200, 250, 300, 400, ···, 1500, 1750, 2000, 2500, 3000, 4000, ···, 10000.

The basic functional form used in GDEM to fit the top 400 m of temperature (top model temperature profile) is the squared amplitude response of a Butterworth filter [*Oppenheim*, 1975]. This expression describes the vertical profile from the surface to the base of the seasonal thermocline ($Z = z_1$). It is then merged with an exponential tail which extends the fit to 400 m ($Z = z_2 = 400$ m). The form of the squared Butterworth response is given by

$$R(Z) = \frac{1}{1 + (Z/A)^{2B}} \tag{1}$$

where Z is the depth ($0 \le Z \le z_1$), A determines the depth of the middle of the thermocline, and B controls the sharpness of the thermocline. Sample curves of $R(Z)$ for two combinations of the coefficients are given in Figure 1. The model curve for the bottom of the top model temperature profile is an exponential function:

$$E(Z) = x^{ax+b} \tag{2}$$

where x is a linear function of Z and $z_1 \le Z \le z_2$. Examples of this function are shown in Figure 2 for various combinations of the coefficients. Although the Butterworth form is nonlinear in terms of the coefficients, it provides the advantage over linear forms of being able to produce smooth functions with only two coefficients. The result can be as steep as necessary without overshooting side lobes.

The base of the thermocline discussed above is defined as the depth past the mixed layer where the vertical gradient of

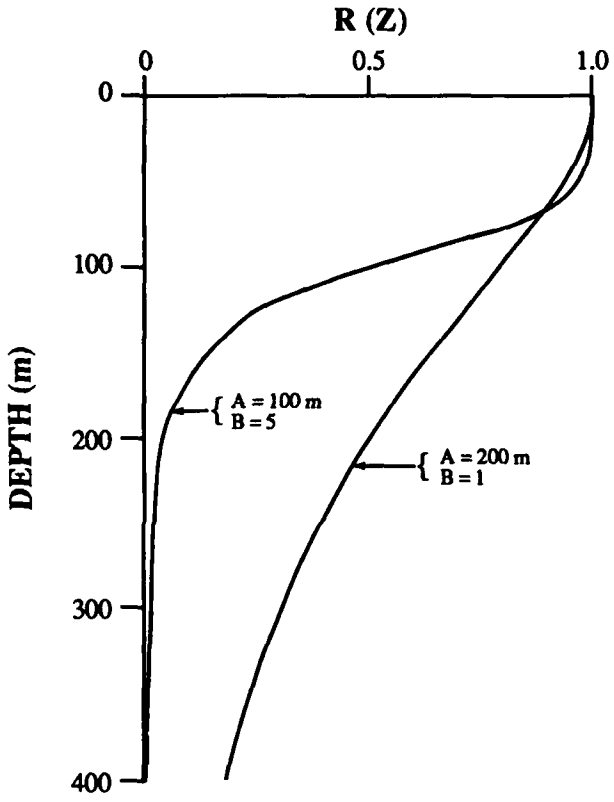

Fig. 1. A squared Butterworth response.

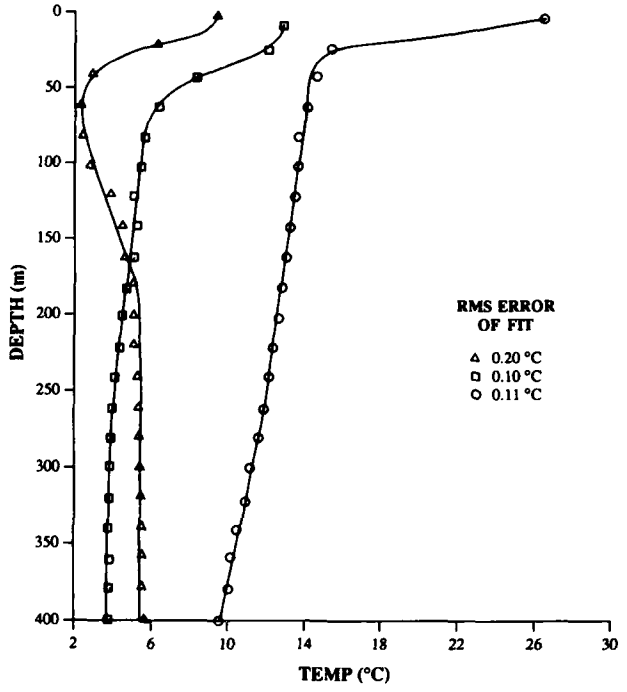

Fig. 3. Examples of the GDEM temperature fit (solid curves) for data (symbols) spanning 0–400 m.

temperature (dT/dZ) is zero. Another definition in use is the depth of the first minimum in slope ($d^2T/dZ^2 = 0$, $dT/dZ < 0$). For the case in the top model region where the tail is not needed, tail coefficients are generated for the depth interval 390–400 m. The exponential tail function is used in lieu of a quadratic function because it allows for changes in sign of d^2T/dZ^2, a condition that is necessary to fit some observed temperature profiles, particularly in the central Pacific.

Combining functions (1) and (2) with appropriate offsets for the Butterworth response and tail yields the fitted temperature,

$$\hat{T}(Z) = \frac{(T_0 - T_{z_1})[1 + (z_1/A)^{2B}]}{[1 + (Z/A)^{2B}](z_1/A)^{2B}} + T_{z_1} - \frac{(T_0 - T_{z_1})}{(z_1/A)^{2B}} \qquad (3)$$

$$0 \le Z \le z_1$$

and

$$\hat{T}(Z) = (T_{z_2} - T_{z_1})x^{ax+b} + T_{z_1} \qquad z_1 \le Z \le z_2 \qquad (4)$$

where $x = (Z - z_1)/(z_2 - z_1)$, T_0 is the temperature at the surface, T_{z_1} is the temperature at depth z_1, and T_{z_2} is the temperature at depth z_2 (400 m). The problem of determining the coefficients for the tail function becomes ill-conditioned when the vertical derivative of temperature approaches 0. This really means that the temperature is constant and is given by

$$\hat{T}(Z) = T_{z_2} \qquad (5)$$

With z_2 set to 400 m the top model consists of eight unknown coefficients (T_0, T_{z_1}, T_{z_2}, z_1, A, B, a, b). The last four coefficients are evaluated utilizing the Gauss-Newton iterative procedure for the least squares solution of nonlinear equations [*Farebrother*, 1988]. This temperature function is fit to each historical temperature profile which passes quality control and editing tests and which falls within the appropriate 3-month time window for the master GDEMs or 1-month windows for the high-resolution and dynamic GDEMs. The rms error of this least squares process is usually much less than 0.5°C. Fits with an rms error greater than 0.5°C are rejected. The adaptive ability of this function to fit various shapes of temperature profiles is shown in Figure 3.

The potentially noisy gridded surface temperature (T_0) monthly fields are smoothed in time using a one-dimensional

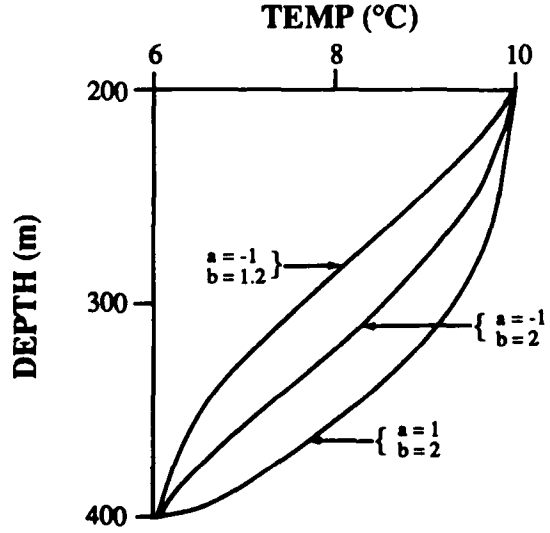

Fig. 2. The exponential tail of the top temperature model.

DTIC
COPY
INSPECTED
A-1 20

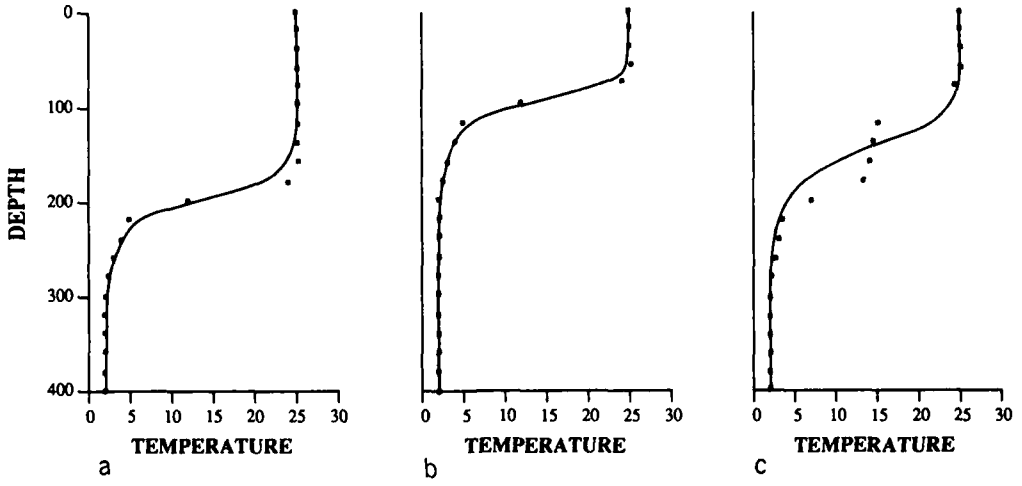

Fig. 4. A comparison of averaging coefficients with averaging observed data values: (*a*) symbol is observed data and line is fit, (*b*) symbol is observed data and line is fit, (*c*) symbol is average of observed data in Figures 4*a* and 4*b* and line is from averaged coefficients.

symmetric low-pass Martin filter [*Martin*, 1957] with a cutoff frequency of 0.2 cycles per month. This filter removes fluctuations with periods less than 3 months. The seasonal sea surface temperature values are derived by averaging the appropriate filtered monthly sea surface temperature values.

Ocean regions as shallow as 100 m can be represented by GDEM, but profiles must first be extended to 400 m for use in the GDEM top model. Profiles which extend to at least 80% of the water depth are extrapolated to 400 m when that local depth is between 100 m and 400 m. Temperature and salinity fields are first built for the entire ocean basin (regardless of depth) using only data that extend to at least 400 m. These fields are then used to control the extrapolation to 400 m of the shallow profiles. Extrapolated profiles are then used to update the GDEM top model. Profiles output from GDEM are considered to be valid to the bottom ($Z \geq 100$ m).

An orthogonal Gram polynomial [*Wylie*, 1975], selected for its ease in computation, is used to fit observed temperature and salinity profiles for the depth range 200–2450 m (middle model profiles) and salinity profiles over the range of 0–400 m (top model salinity profile). The attractiveness of using orthogonal polynomial expansions is that computation

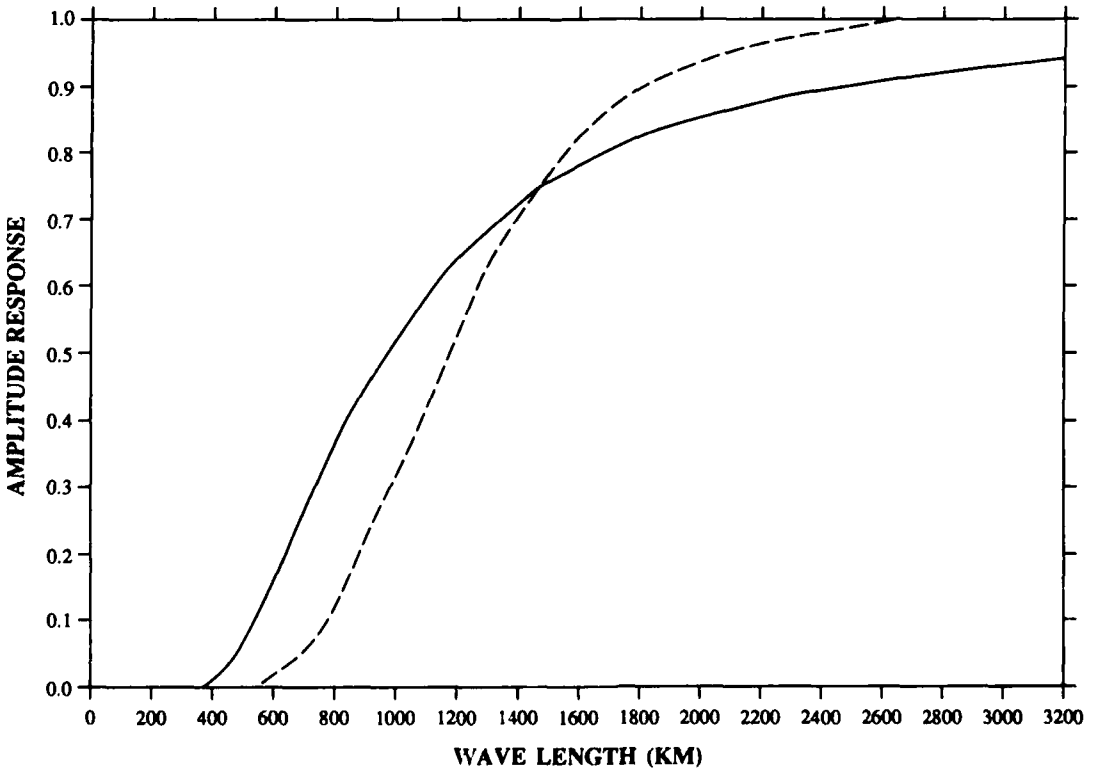

Fig. 5. Response function for GDEM (solid) and LC (dashed) horizontal smoothing.

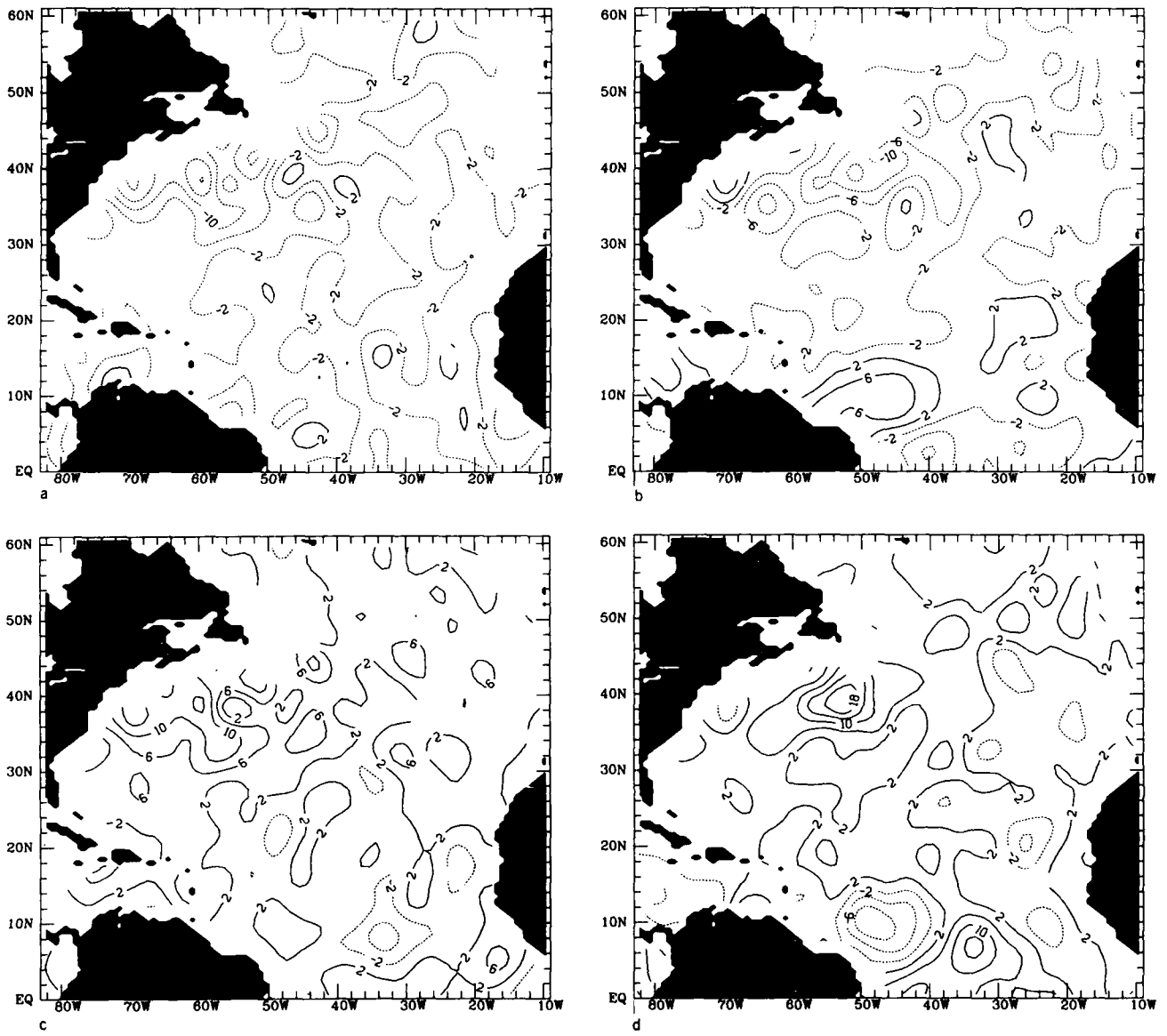

Fig. 6. GDEM seasonal anomalies in dynamic height (smoothed) for the North Atlantic: (*a*) winter − annual, (*b*) spring − annual, (*c*) summer − annual, and (*d*) fall − annual. The contour interval is 4 dyn cm.

of higher-order coefficients does not require recomputation of the lower-order coefficients. Orthogonal polynomials are given by

$$P_{NM}(D) = \sum_{K=0}^{M} (-1)^K \binom{M}{K} \binom{M+K}{K} \frac{D^K}{N^K} \qquad (6)$$

for degree $M = 0, 1, 2, \cdots, N$.

The functional form of the orthogonal polynomial expansion is

$$\hat{G}(D) = a_0 P_{N0}(D) + a_1 P_{N1}(D) + \cdots a_M P_{NM}(D) \qquad (7)$$

where G can represent either temperature or salinity. Interpolation of data to evenly spaced intervals prior to fitting the orthogonal polynomial improves the mathematical stability of the process to determine the polynomial coefficients. D represents the depth index; $D = 1, 2, \cdots, N$ for the evenly spaced temperature or salinity data (see Table 1). The relationship for the coefficients is given in a form that is easy to use in least squares determinations by

$$a_K = \frac{\sum_{D=0}^{N} G(D) P_{NK}(D)}{\sum_{D=0}^{N} P_{NK}^2(D)} \qquad (8)$$

for $K = 0, 1, 2, \cdots, M$.

In order to determine the degree of the polynomial required to model the observed temperature and salinity profiles, measured profiles were selected which exhibited a large amount of vertical variability. The maximum allowed rms error of fit is 0.1‰ for the top salinity model, 0.05‰ for the middle salinity model, and 0.25°C for the middle temperature model. The appropriate degree of the fit is selected by observing when the rms error curves begin to flatten out and

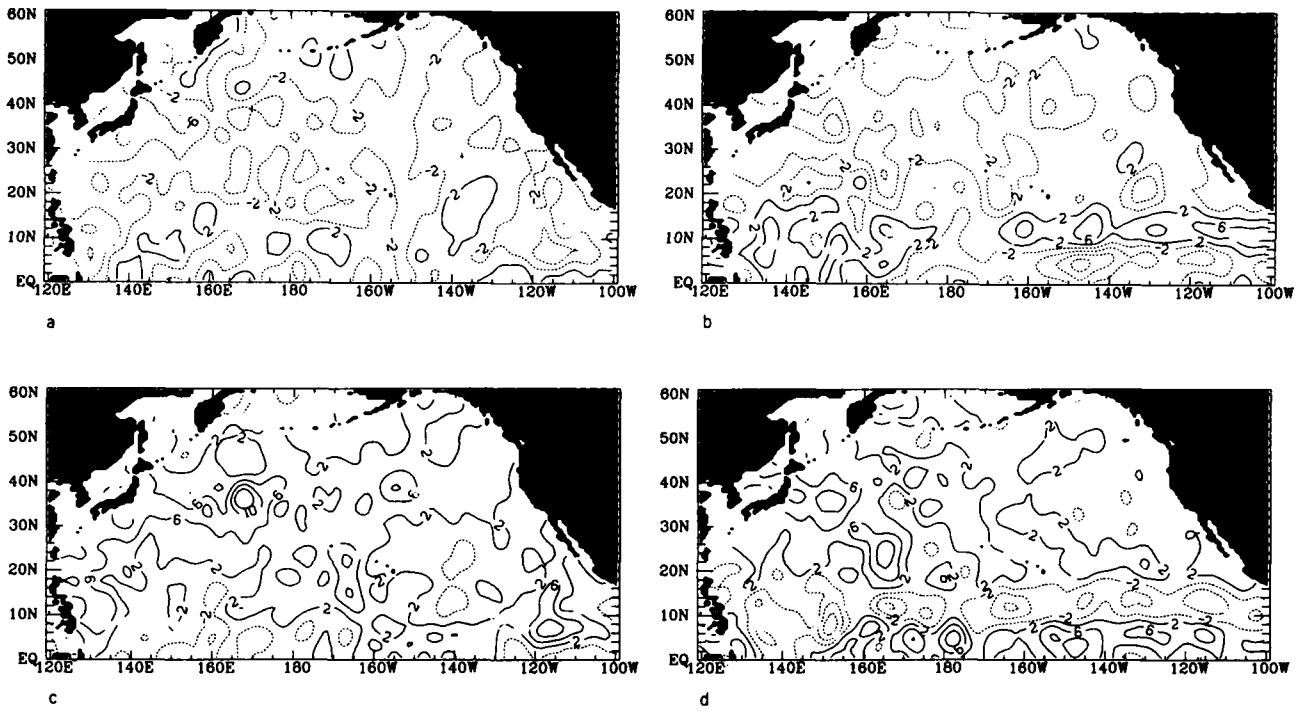

Fig. 7. GDEM seasonal anomalies in dynamic height (smoothed) for the North Pacific: (*a*) winter − annual, (*b*) spring − annual, (*c*) summer − annual, and (*d*) fall − annual. The contour interval is 4 dyn cm.

trading that measure off with the desire to use the lowest degree possible in order to minimize rippling in the more stable regions of the profiles. These considerations resulted in the selection of five degrees ($M = 5$) for the top and middle salinity models and seven degrees ($M = 7$) for the middle temperature model.

The deep temperature and salinity profiles (deep model profile) are least squares fitted to a simple quadratic polynomial

$$F(Z) = c_1 + c_2 Z + c_3 Z^2 \tag{9}$$

for $2000 \leq Z \leq$ bottom depth. This form typically fits the observed temperature profiles with an rms error of less than 0.25°C and the deep salinity profiles with an rms error of less than 0.05‰.

After the functional-form coefficients are computed for each data profile, a uniform spatial grid of coefficients is produced for each one. This processing utilizes a two-dimensional, multistage, minimum-curvature least squares spline [after *Briggs*, 1984; *Swain*, 1976; *Gonzalez-Casanova and Alvarez*, 1985] which has been designed to minimize spatial aliasing while preserving the continuity of the derivatives in all three space dimensions. The advantages of utilizing interpolated temporal and spatial grids of coefficients of appropriate one-dimensional functional forms rather than gridding values of the observed temperature and salinity at selected depths is illustrated in Figure 4 using the top temperature model. The process of averaging the input data at each depth tends to result in a distorted profile which is not representative of either of the observed profiles. However, averaging the coefficients results in a realistic profile which matches the shape of the input data and places the thermocline at the average depth.

These coefficient grids are used to calculate both modeled temperature and salinity for each grid point at standard depths for each submodel. In merging together the top and middle model profiles, a correction is applied to each. If the difference in temperature at 400 m is less than 0.25°C, then only the middle model profile is modified by adding the differences to the top values of the middle profile (enforcing temperature continuity). If the difference is larger than 0.25°C, then the top model profile is changed as well, absorbing half of the difference. One further refinement occurs when the difference in temperature at 400 m is greater than 1.0°C. The top model profile then absorbs all the difference in excess of 0.5°C. The top model profile is modified from 400 m upward, and the middle model profile is modified from 400 m downward. The modification technique (adapted from *Boston* [1987]), which is used to correct the profiles (not the coefficients), is the same for each profile, except that the top model modification decays more rapidly. The corrected temperature at any given depth Z is

$$T_{\text{new}} = T_Z + \alpha \Delta T (0.835)^{\beta} \tag{10}$$

for $\beta = \delta |Z - \text{merge depth}|$, where T_{new} is the merged temperature and T_Z is the model temperature at depth Z. The difference in temperature at merge depth, ΔT, is $T_{\text{mid}} - T_{\text{top}}$ for the top merge and $T_{\text{top}} - T_{\text{mid}}$ for the middle merge. The percent ΔT assigned to the merge is α, and the scaling factor δ is 0.01 for the middle model and 0.05 for the top model. The decay factor (0.835) was determined empirically to allow the ΔT to decay to the generally accepted level of no motion (2000 m).

After the upper merge (top model and middle model) for the master GDEM is made, the merged values for 400 and 500 m are removed, and a cubic spline is fit to the remaining values from the surface to the bottom of the middle model. New interpolated values for 400 and 500 m are estimated by

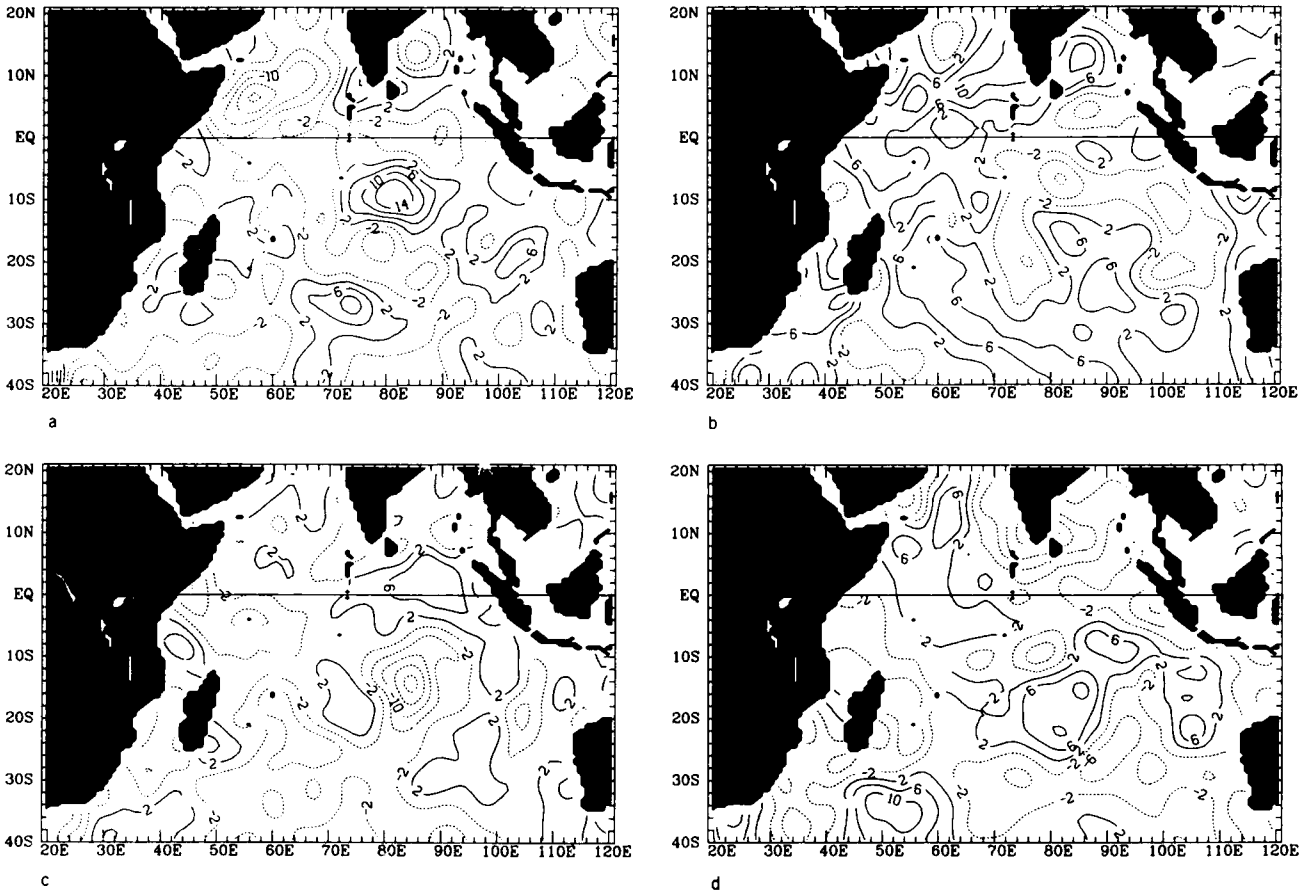

Fig. 8. GDEM seasonal anomalies in dynamic height (smoothed) for the Indian Ocean: (*a*) winter − annual, (*b*) spring −annual, (*c*) summer − annual, and (*d*) fall − annual. The contour interval is 4 dyn cm.

evaluating the spline at those depths. This procedure ensures that the first and second derivatives of the profile are continuous at the merged depth.

The merge between the middle and deep models is similar to the upper merge, except the difference is taken at 2000 m, and the correction is applied upward from 2000 m on the middle model profile. The correction decays twice as fast as the downward correction of the upper merge ($\delta = 0.02$). This merge is actually done before the upper merge, and the corrections are always small. Differences between the top and middle models before the merge at merge depth in the North Atlantic for summer (which are similar to differences for other seasons) for grid cells with GDEM profiles (16,091) were less than 1.0°C for 88% of the time and were less than 0.2‰ for 94% percent of the time.

Each monthly surface temperature value is stored in GDEM for use in an intermonthly interpolation scheme. Intermonthly interpolation is accomplished by linearly interpolating in time between the coefficients of the appropriate seasonal temperature profiles for their new "top model" coefficients, except for T_0 and T_{S_2}. In the case of the T_{S_2} coefficient the seasonal value nearest in time to the desired time is used. This step ensures that the resulting temperature profile will be continuous from the surface to the bottom. In the case of the T_0 coefficient, the two adjacent (in time) monthly surface temperature values from the low-pass-filtered data are linearly interpolated in time to the appropriate value (month, week, day, etc.) and are used as the new T_0. The new (interpolated) coefficients are then used to compute the temperature profile.

Each of the dynamic GDEMs presently consists of two 30′ × 30′ GDEMs, one representing the cold water mass found north of the major front and the second representing the warm water mass found south of the major front. If a reasonable estimate of the position of the front for a particular time is known, then the cold-water GDEM can be used north of the front, and the warm-water GDEM can be used south of the front. The two data bases can be connected with a "feature model," i.e., a model of the front (similar to that of *Kao* [1987]) which is embedded on the grid between the two GDEMs at an estimated front location (may be determined by infrared (IR) imagery or altimetry, for example). If one knows the position and geometry of the associated rings, then ring feature models can be embedded in the model as well. The final result is a three-dimensional model of temperature, salinity, and sound speed for the analysis period at a resolution that adequately represents the gradients of the features.

Anticipated future developments at NAVOCEANO include improvements to the analytical forms used to compute coefficients, a shallow water GDEM for regions shallower than 400 m, a three-water mass dynamic GDEM for the North Pacific Ocean north of 30°N, and a model which will contain estimates of variability in temperature and of associated acoustical features as functions of depth for each GDEM grid cell. Methods for embedding near-real-time data

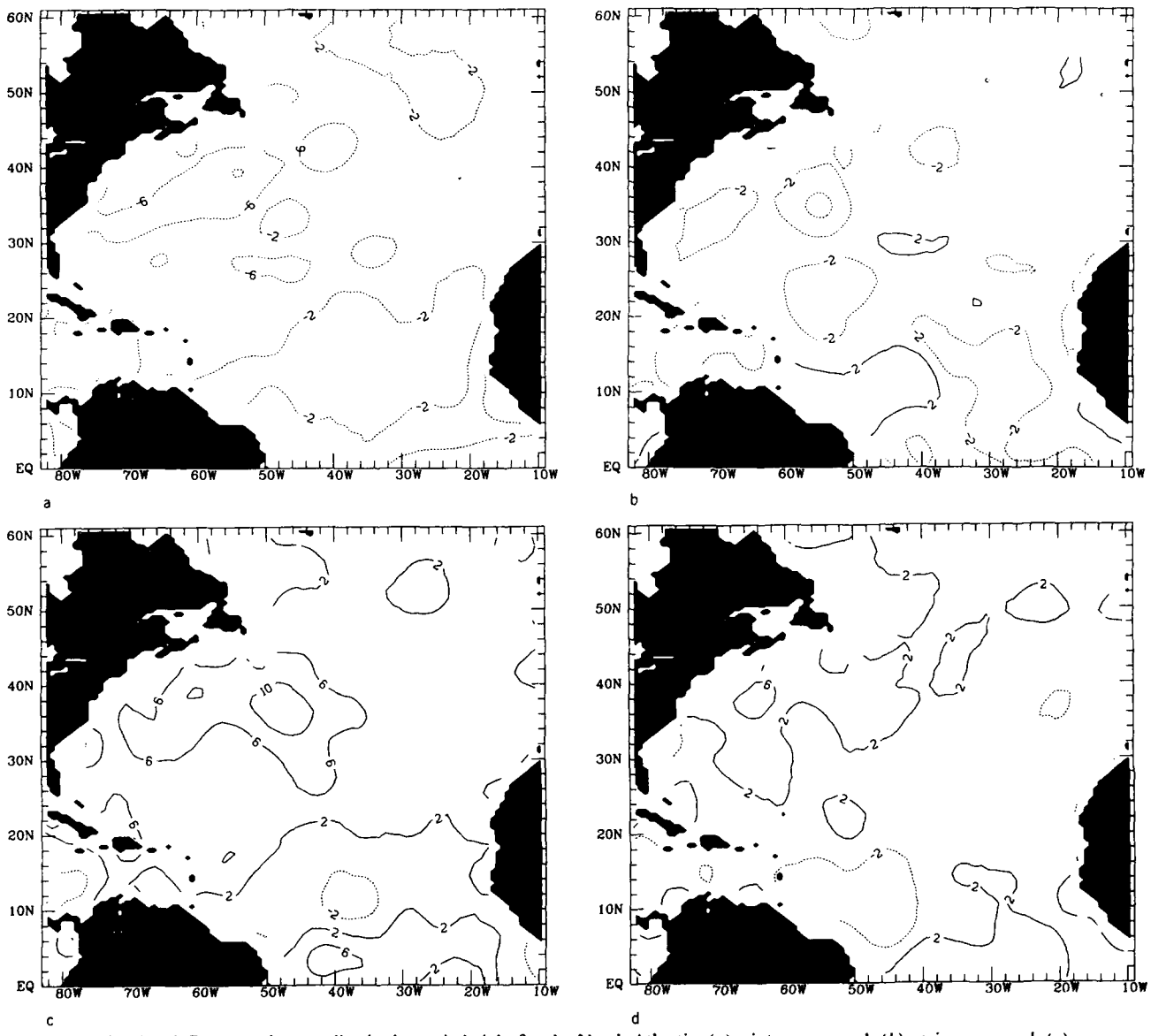

Fig. 9. LC seasonal anomalies in dynamic height for the North Atlantic: (*a*) winter − annual, (*b*) spring −annual, (*c*) summer − annual, and (*d*) fall − annual. The contour interval is 4 dyn cm.

in GDEM from sources such as expendable bathythermographs, radiometer IR imagery, and satellite altimetry are also being developed for improving the climatological representations for particular time periods.

3. LC Description

LC consists of objectively analyzed fields of temperature, salinity, dissolved oxygen, and percent oxygen saturation (oxygen will not be described here). Temperature and salinity fields were prepared from all available data regardless of the year of observation, because synoptic data for individual years were not available. There were large variations in both spatial and temporal aspects of the data distribution. Data amounts decrease in the Levitus analysis with increasing depth. The 1.6 million profiles which were used for the analysis consisted of all data available in the NODC oceanographic station data file as of the first quarter of 1978 and in the expendable bathythermograph and mechanical bathythermograph files as of the first quarter of 1977. The data were screened and subjected to quality control procedures which included range checks, static stability checks, and various statistical checks. Obviously erroneous, duplicate, and nonrepresentative data were eliminated. The edited data were averaged into values for 1° squares for input to the objective analysis scheme.

The resulting temperature and salinity fields were generated by means of an iterative difference-correction scheme [*Cressman*, 1959]. The observed 1° square averages from all available data for the season being analyzed (regardless of the year) and a first-guess value for each square were included in the objective analysis. The same analysis scheme was used for all levels. It is described in further detail in the atlas [*Levitus*, 1982].

A quick sketch of the scheme follows. The temperature and salinity values for each 1° square value were located on the grid at the center of that particular square. Thus the 360

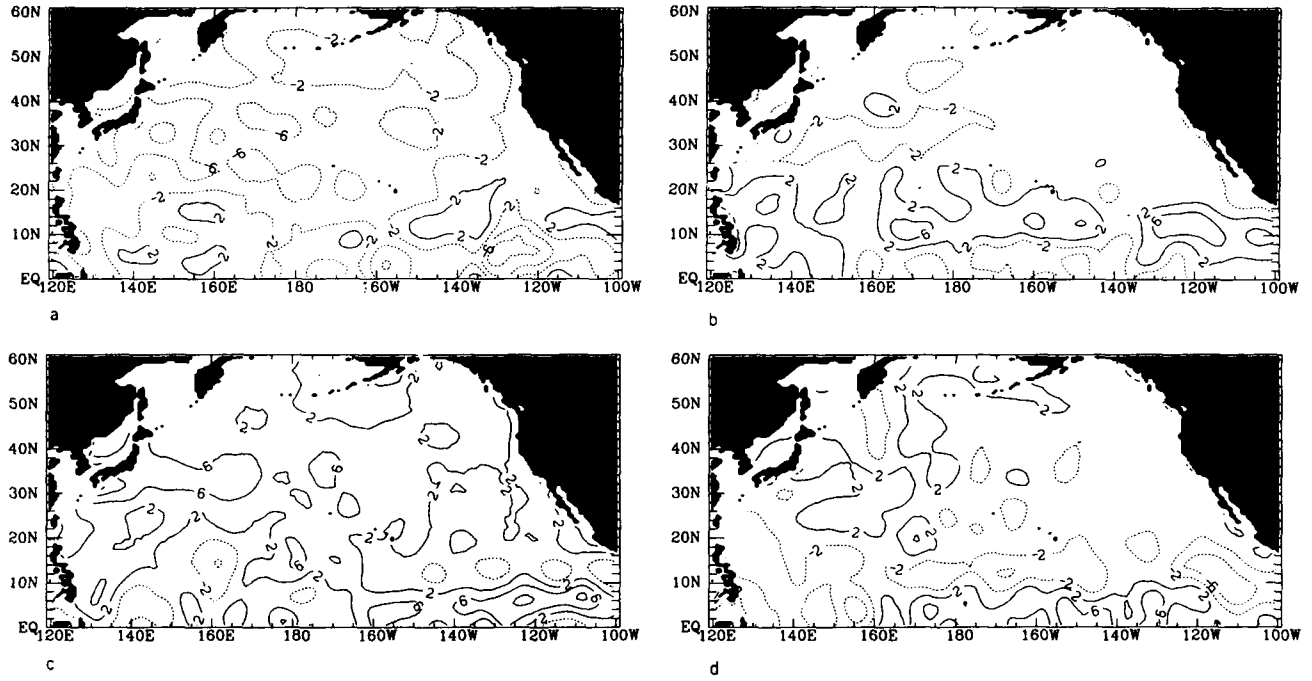

Fig. 10. LC seasonal anomalies in dynamic height for the North Pacific: (*a*) winter − annual, (*b*) spring −annual, (*c*) summer − annual, and (*d*) fall − annual. The contour interval is 4 dyn cm.

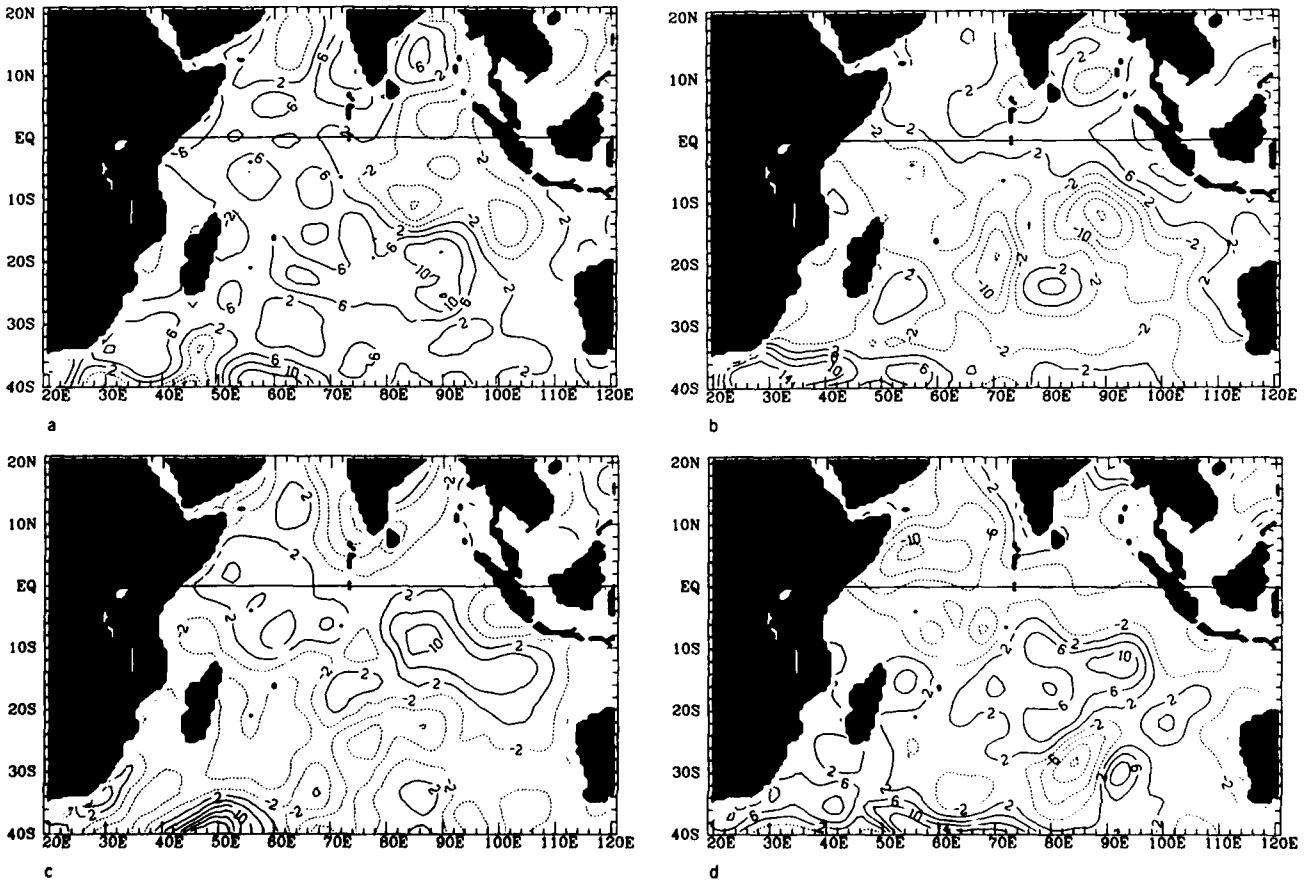

Fig. 11. LC seasonal anomalies in dynamic height for the Indian Ocean: (*a*) winter − annual, (*b*) spring −annual, (*c*) summer − annual, and (*d*) fall − annual. The contour interval is 4 dyn cm.

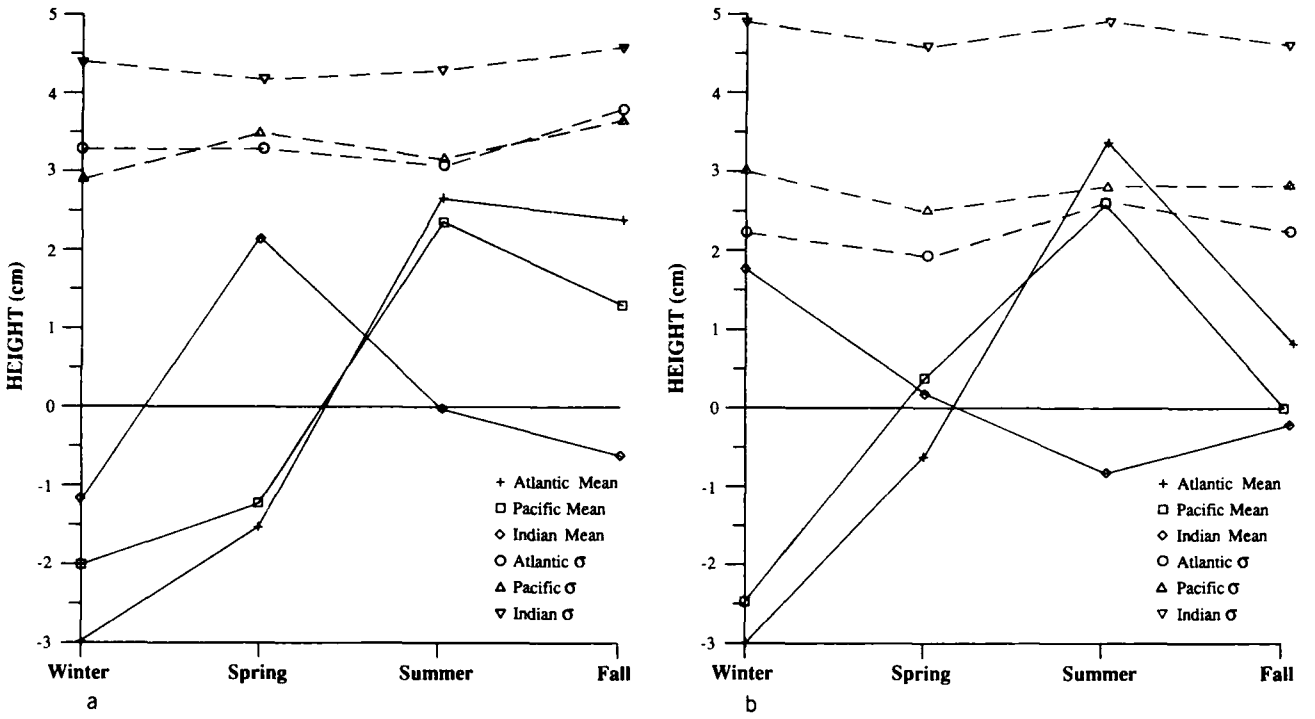

Fig. 12. Basin-wide mean values of dynamic height seasonal anomalies (seasonal value minus annual mean value) and their standard deviations (σ) for the Atlantic, Pacific, and Indian Oceans: (*a*) smoothed GDEM and (*b*) LC.

× 180 grid points in the LC are located at the intersection of the $\frac{1}{2}°$ lines of latitude and longitude. A first guess of temperature and salinity for each grid square within a 1° latitude zone across individual ocean basins was made by averaging all observed data within that zone. A correction to the first-guess value for a grid square was computed as a distance-weighted mean of the differences between the first-guess field and the mean values (where they could be computed). The differences used in this objective analysis scheme were computed within an area around the grid point defined by an influence radius. A fixed set of influence radii was used so that each parameter at every depth for each season could be analyzed in the same manner. At each grid point, new, analyzed values of temperature and salinity, consisting of the sum of the first guess and the correction, were computed. If there were no data within the influence radius of a given grid point, the analyzed value at that grid point was taken as the first-guess value. The procedure consisted of four iterations applied to the first guess field, where influence radii were 1541, 1211, 881, and 771 km. Energy at wavelengths less than 700 km in the updated field was substantially reduced. After each iteration the resulting field was smoothed with a five-point filter of the type described by *Schuman* [1957] chosen to approximate the response function of the objective analysis scheme. The amount of smoothing in the objective analysis with four iterations and the five-point filter applied after each pass is shown by the response function in Figure 5.

4. Intercomparison Methods

GDEM and LC dynamic height fields for the North Atlantic and North Pacific oceans were computed for each season and for the annual mean. GDEM seasons for the Indian Ocean are based on monsoon periods and are quite different from the seasons used by LC. Hence fields were computed only for the annual mean for the Indian Ocean. Dynamic heights relative to a reference level of 1000 m were computed where water depths reached this reference level. Differences between GDEM and LC dynamic height fields were computed for seasonal and annual means for the North Atlantic and North Pacific oceans and for the annual mean for the Indian Ocean. The units of dynamic height, dynamic centimeters (10 dyn cm = 1 J/kg), will be hereafter referred to in this paper as centimeters, for simplicity.

GDEM seasons for the North Atlantic and North Pacific are winter (January–March), spring (April–June), summer (July–September), and fall (October–December). GDEM seasons for the Indian Ocean are winter monsoon (mid-October through February), spring transition (March through mid-May), summer monsoon (mid-May through mid-July), and fall transition (mid-July through mid-October). LC seasons for the entire world are winter (February–April), spring (May–July), summer (August–October), and fall (November–January). Despite differences in averaging periods, the comparisons of the difference fields are quite meaningful, since there is a 67% overlap in seasons and since LC is so heavily smoothed in time and space.

Horizontal spatial resolution of GDEM is $\frac{1}{2}°$ by $\frac{1}{2}°$ while LC spatial resolution is 1° by 1°. Vertical resolution of GDEM was made the same as LC by outputting the GDEM fields at the standard levels used in LC. For comparison purposes we have applied comparable smoothing to GDEM dynamic height fields to make the wave number spectrum compatible with that of LC. This smoothing was applied to GDEM fields on the $\frac{1}{2}°$ grid with a three by three point filter (center weight of $\frac{1}{4}$, normal-line weights of $\frac{1}{8}$, and diagonal-line weights

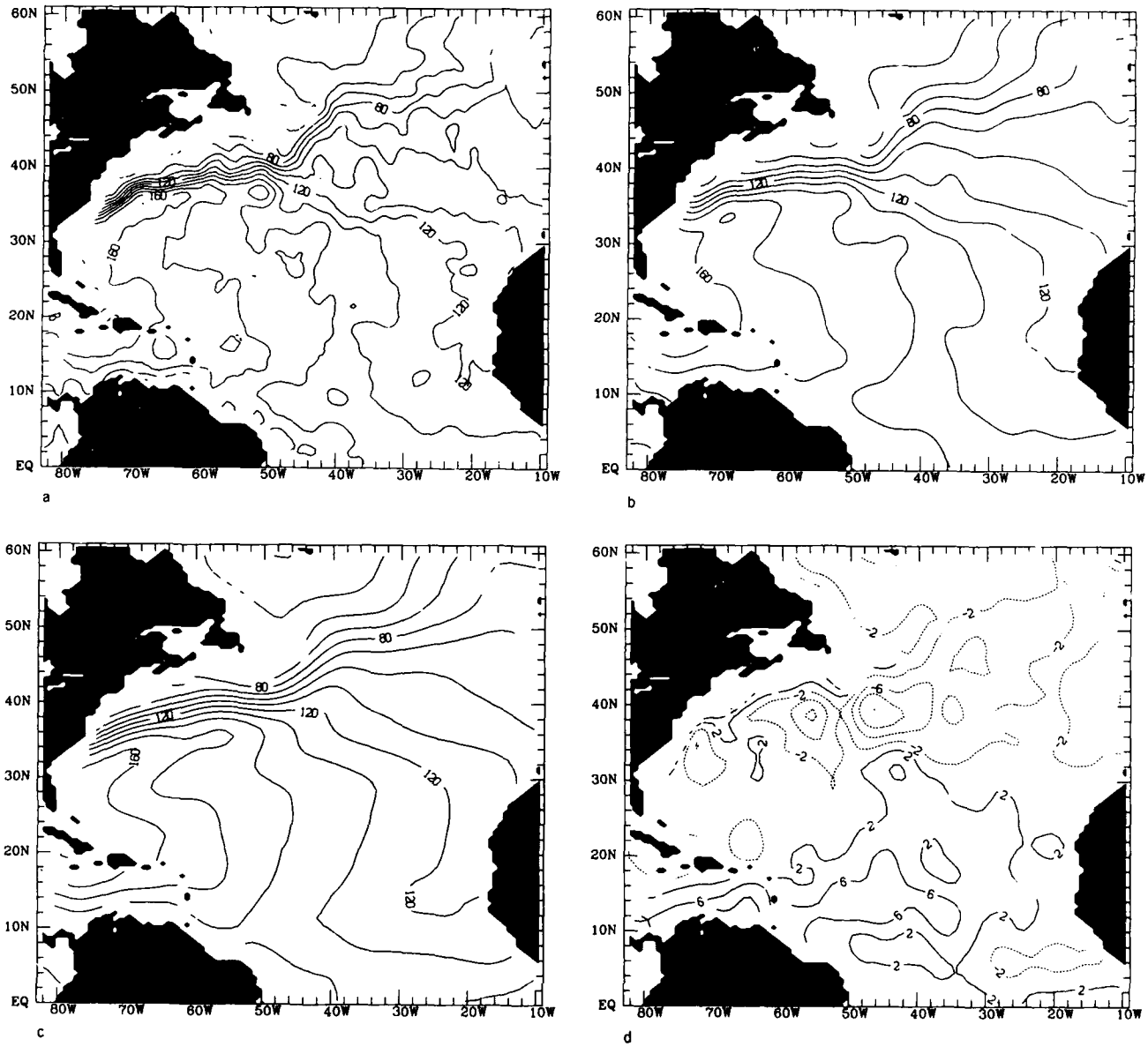

Fig. 13. North Atlantic annual mean dynamic height: (*a*) GDEM, (*b*) GDEM smoothed, (*c*) LC, (*d*) smoothed GDEM − LC. The contour interval is 10 dyn cm for Figures 13*a*–13*c* and 4 dyn cm for Figure 13*d*.

of $\frac{1}{16}$) with weights modified to reflect the changing distance between meridians on a latitude-longitude grid. For simplicity the amount of GDEM smoothing is controlled by the number of filter applications. GDEM dynamic heights were filtered 20 times successively to produce smooth fields that were comparable in spectral content to LC fields. The response of this filter when applied 20 times is shown in Figure 5. The half-amplitude point of the smoothing filter used in the LC analysis occurs at about 1200 km (almost 11° of latitude), while the half-amplitude point for the filter used in the additional smoothing of GDEM occurs at about 1000 km.

GDEM was subsampled at the same grid points as those used in LC before the comparisons were made between LC- and GDEM-derived fields. Comparisons using both smoothed and unsmoothed GDEM dynamic height fields are discussed. Differences are often significantly greater between LC and unsmoothed GDEM fields than between LC and smoothed GDEM fields.

5. Seasonal Anomaly

Seasonal anomalies are computed for each climatology by subtracting the annual mean from the seasonal fields. GDEM seasonal anomaly maps were prepared only from the smoothed GDEM fields. Seasonal anomalies computed from unsmoothed GDEM have peak values about 30% higher than those of the smoothed fields. GDEM seasonal anomaly maps are shown for the Atlantic in Figure 6, for the Pacific in Figure 7, and for the Indian Ocean in Figure 8 (the seasonal anomaly for the Indian Ocean cannot be directly compared with LC because of the incompatibility in the defined season periods).

Greatest GDEM seasonal anomalies in the Atlantic were

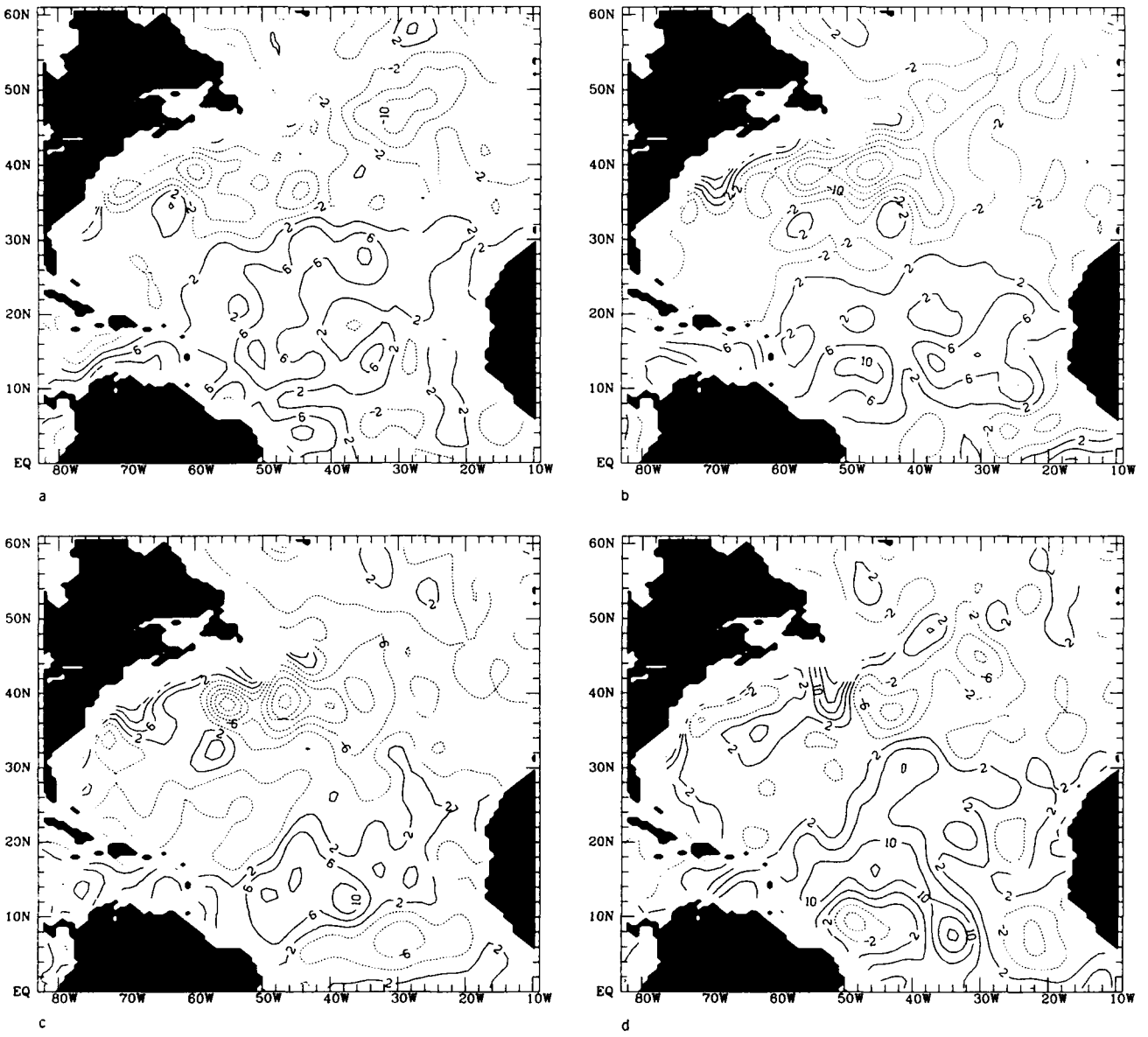

Fig. 14. North Atlantic seasonal dynamic height differences between smoothed GDEM and LC: (*a*) winter, (*b*) spring, (*c*) summer, and (*d*) fall. The contour interval is 4 dyn cm.

found in the Gulf Stream region and ranged to almost 20 cm for winter and fall. Anomalies ranged from about 5 cm for spring to −10 cm for fall in a region off northeastern South America in the equatorial current region near 10°N, 50°W. Seasonal anomalies in the Sargasso Sea were generally 5 cm or less. Winter and spring anomalies for the Gulf Stream were negative, while summer and fall anomalies were positive.

Seasonal anomaly magnitudes for the Kuroshio were generally less than those for the Gulf Stream. They were typically 5–10 cm except near 170°E, where they were almost 15 cm for the summer. Similar to the Gulf Stream anomalies, winter and spring anomalies for the Kuroshio were negative, and summer and fall anomalies were positive. Seasonal anomaly magnitudes of 5–10 cm were common in the Pacific equatorial region. Anomaly magnitudes were usually less than 5 cm in the northeast Pacific.

In the Indian Ocean near the confluence region of the South Equatorial Current and the Equatorial Countercurrent (near 10°S, 85°E), a large anomaly of about 15 cm occurs during the winter monsoon season, while an anomaly of about −15 cm occurs during the summer monsoon season. During spring and fall transition seasons this anomaly is considerably weakened. Anomaly magnitudes greater than 10 cm are found in the Arabian Sea (northwestern Indian Ocean) during winter and spring and in the Agulhas Current (extreme southwestern Indian Ocean) during all seasons. Elsewhere, anomaly magnitudes are generally 5 cm or less.

Corresponding LC maps of seasonal anomalies are shown for the Atlantic and Pacific in Figures 9 and 10. LC seasonal anomalies for the Indian Ocean, which cannot be directly compared with GDEM, are shown in Figure 11. Anomaly magnitudes are generally much less than 5 cm in both the Pacific and the Atlantic. Much larger seasonal anomalies are found in the Indian Ocean. Magnitudes greater than 10 cm are found in the central basin in the equatorial current

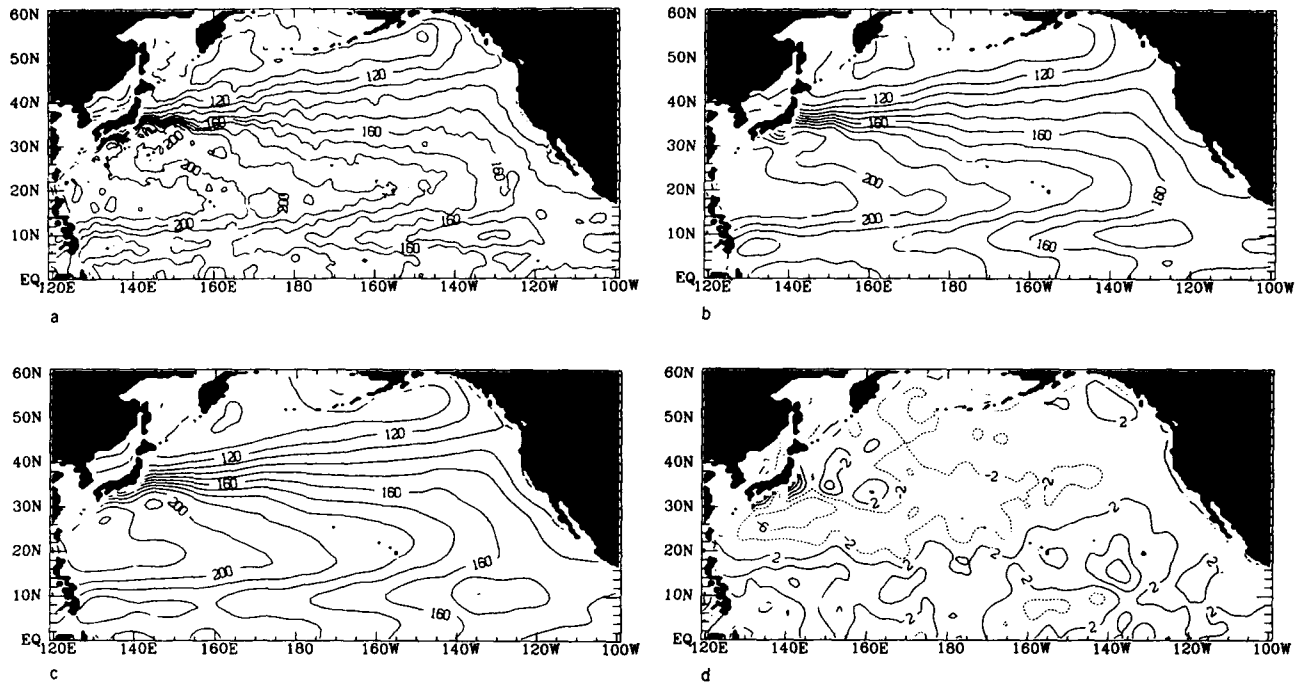

Fig. 15. North Pacific annual mean dynamic height: (*a*) GDEM, (*b*) GDEM smoothed, (*c*) LC, and (*d*) smoothed GDEM − LC. The contour interval is 10 dyn cm for Figures 15*a*–15*c* and 4 dyn cm for Figure 15*d*.

region, near the Agulhas Current, and in the southwestern region near 40°S. Elsewhere in the Indian Ocean, magnitudes were generally less than 10 cm.

Basin-wide mean seasonal anomalies computed from the smoothed GDEM for the Pacific and Atlantic range from a high of 2–3 cm in summer to a low of −2 to −3 cm in winter with a standard deviation of 3–4 cm in each season for each basin (Figure 12*a*). However, the fall means are only slightly smaller than the summer means, and spring means are only slightly larger than the winter means. The mean GDEM seasonal anomaly for the Indian Ocean ranges from 0 to −1 cm, except for spring, when the mean is about 2 cm, with a standard deviation of about 4.5 cm for all seasons. The mean values are the same for the cases of both smoothed and unsmoothed fields, but standard deviations are about 1 cm higher for the latter.

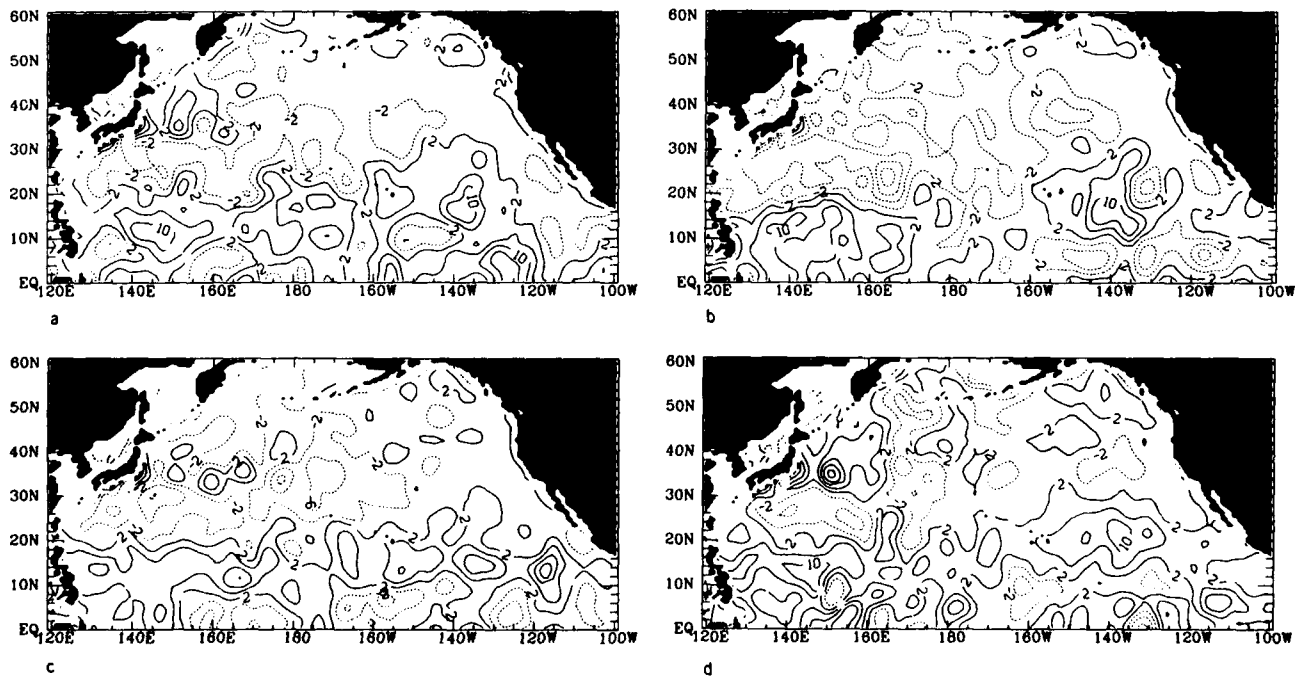

Fig. 16. North Pacific seasonal dynamic height differences between smoothed GDEM and LC: (*a*) winter, (*b*) spring, (*c*) summer, and (*d*) fall. The contour interval is 4 dyn cm.

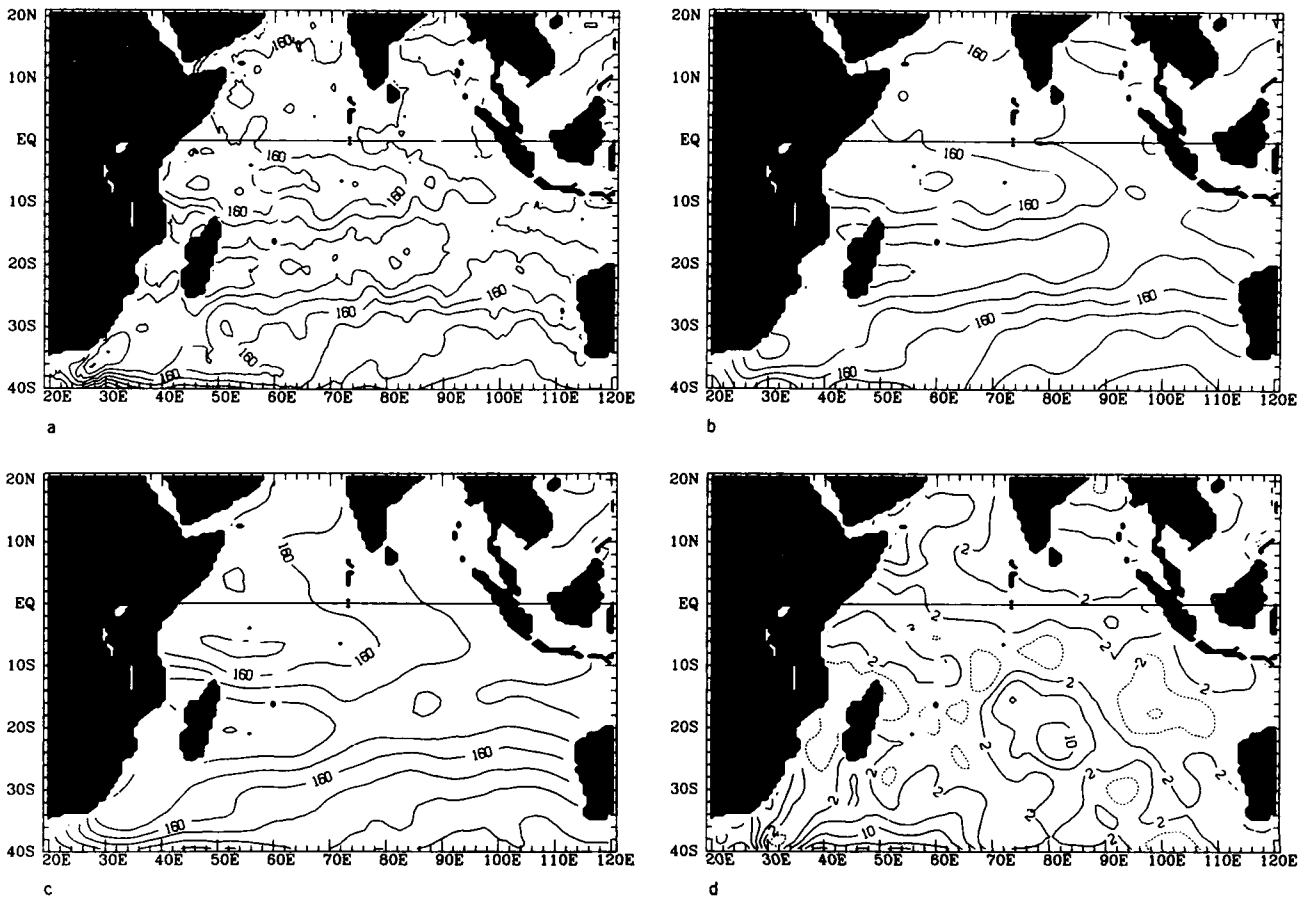

Fig. 17. Indian Ocean annual mean dynamic height: (*a*) GDEM, (*b*) GDEM smoothed, (*c*) LC, and (*d*) smoothed GDEM − LC. The contour interval is 10 dyn cm for Figures 17*a*–17*c* and 4 dyn cm for Figure 17*d*.

Basin-wide mean seasonal anomalies from LC for the Pacific and Atlantic range (similarly to GDEM) from a high of 2–3 cm in summer to a low of −2 to −3 cm in winter (Figure 12*b*), with standard deviations of 2–3 cm. However, mean LC seasonal anomalies for spring and fall are about midway between winter and summer, which is reflective of the smoothing in time as well as of the somewhat different season definitions. Although the seasons are defined differently in LC and GDEM, mean LC seasonal anomalies for the Indian Ocean range similarly to those for GDEM, from 0 to −1 cm, except for winter, when the mean is about 2 cm, with a standard deviation of about 4.5 cm.

6. Dynamic Height Differences

Differences in dynamic height fields between GDEM and LC were computed for each season and annual mean for the Pacific and Atlantic oceans and for the annual mean for the Indian Ocean (Figures 13–17). Difference magnitudes ranged up to about 50% higher when using the unsmoothed GDEM than when using the smoothed GDEM. For the annual mean cases, unsmoothed GDEM fields, smoothed GDEM fields, and LC fields are shown along with the differences between LC and smoothed GDEM fields. For the seasonal cases, only differences between LC and smoothed GDEM fields are shown.

The annual mean dynamic height field of the smoothed GDEM (Figure 13*b*) for the Atlantic Ocean is quite similar in appearance to the LC field (Figure 13*c*). As expected, the largest differences, about −10 cm, are found in the Gulf Stream region (Figure 13*d*). Elsewhere, differences are generally less than 5 cm. However, the unsmoothed GDEM (Figure 13*a*) is noticeably different from LC, particularly in the Gulf Stream region. The width of the current-shear region in GDEM is about half that of LC. Furthermore, there is a standing Gulf Stream meander in GDEM which has been smoothed out in LC. Differences between unsmoothed GDEM and LC range to about −20 cm in the Gulf Stream region, while outside the Gulf Stream, differences are less than 10 cm.

Seasonal dynamic height field differences between smoothed GDEM and LC for the Atlantic Ocean (Figure 14) are 10–15 cm larger in magnitude than the annual differences in the Gulf Stream region. Elsewhere, seasonal height field differences computed using the smoothed GDEM are generally less than 10 cm. Two minimums in the spring and summer height difference fields in the Gulf Stream region are also seen in the annual difference fields. Seasonal differences range from about −20 to 20 cm when using the smoothed GDEM and almost twice that when using the unsmoothed GDEM. The largest differences between GDEM and LC height fields are found in the Gulf Stream region.

For the Pacific Ocean (Figure 15) the annual mean dynamic height field of the smoothed GDEM is much like the annual field of LC. Differences between smoothed GDEM

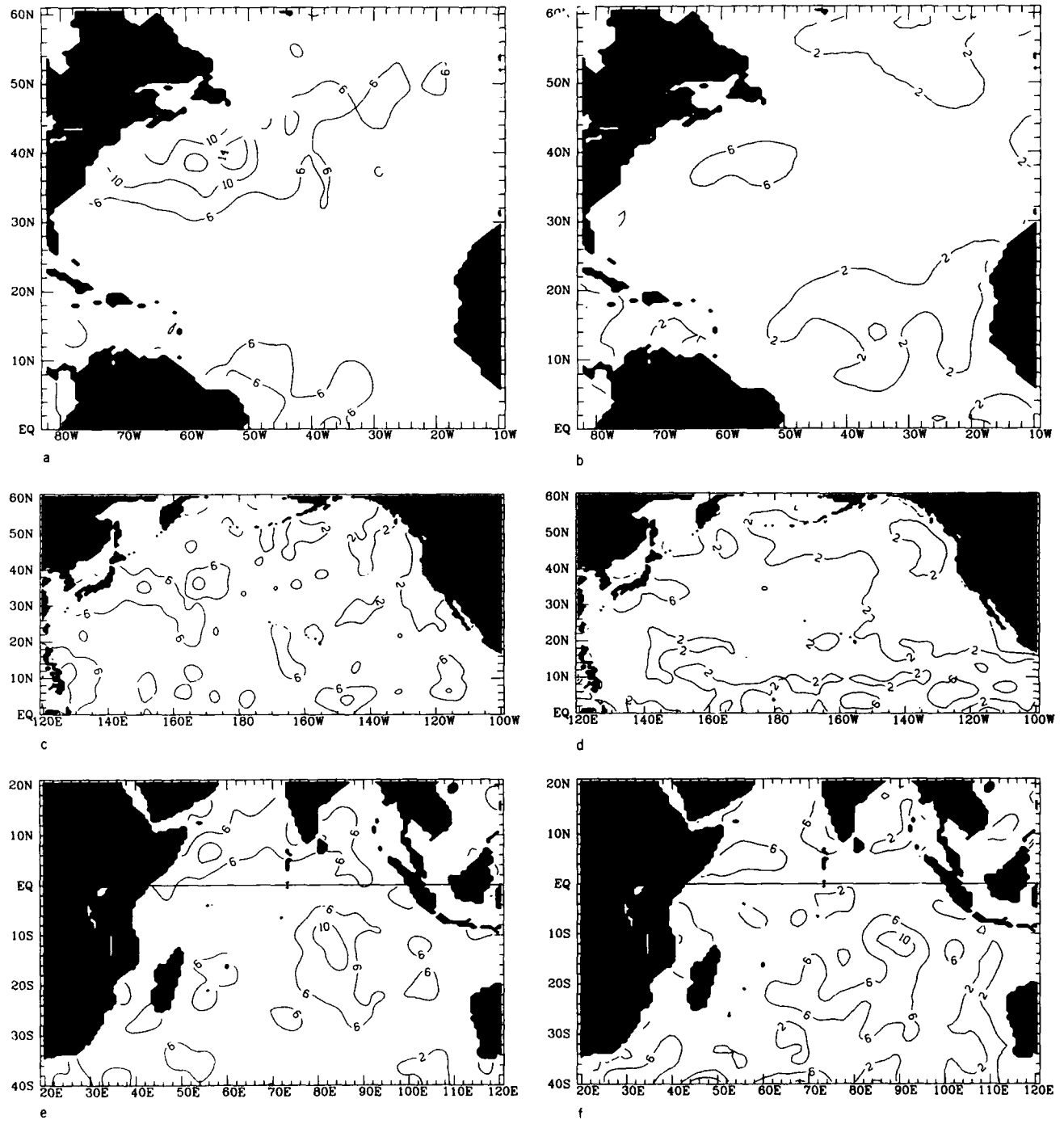

Fig. 18. North Atlantic rms variability: (*a*) smoothed GDEM and (*b*) LC. North Pacific rms variability: (*c*) smoothed GDEM and (*d*) LC. Indian Ocean rms variability: (*e*) smoothed GDEM and (*f*) LC. The contour interval is 4 dyn cm.

and LC are in general 5 cm or less and are somewhat higher when using unsmoothed GDEM. Annual mean differences of about 10 cm are found in a section of the Kuroshio. Greater differences are apparent in the seasonal dynamic height fields (Figure 16). The largest differences (about 15 cm using the smoothed GDEM) are found in the zone defined by the equator and 20°N and in the Kuroshio region. Very good agreement, less than 5 cm differences for the smoothed GDEM case, is found in the northeast Pacific for all seasons.

The LC height field for the Indian Ocean generally agrees with the GDEM height field for the annual case (Figure 17). Differences of 10–15 cm are found in the central Indian Ocean. The largest differences are in the vicinity of the Agulhas Current and near 40°S, between 20°E and 60°E: about 15 cm when differencing the smoothed GDEM and twice that when using the unsmoothed GDEM.

7. Discussion and Summary

We have shown some similarities and differences between GDEM and LC. The characters of these climatologies are

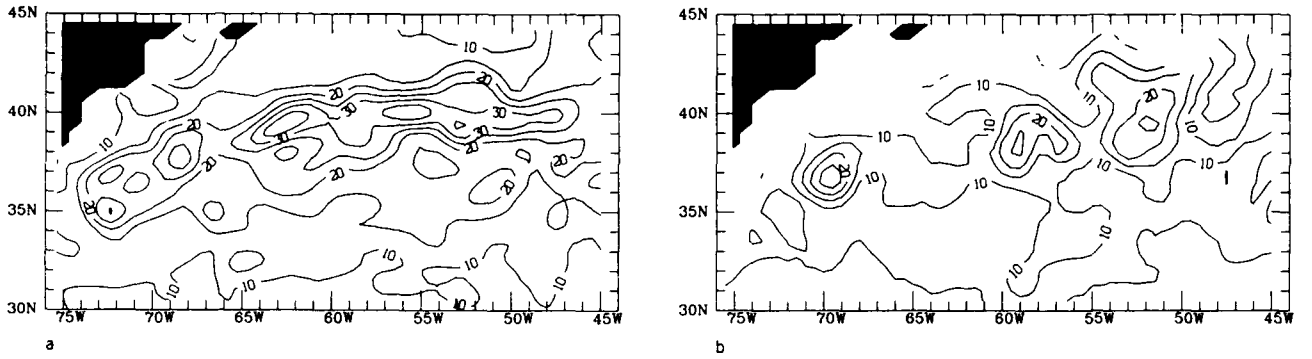

Fig. 19. Gulf Stream region rms variability from (*a*) GEOSAT altimetry and (*b*) GDEM. The contour interval is 5 cm.

quite different, primarily for two reasons. First, the 1.6 million profiles used in the construction of LC were only part of the 4 million profiles used in the formation of GDEM. Second, mean fields in LC are obtained through an objective analysis of temperature and salinity data, whereas in GDEM, analytic functions are fitted to individual observations, and the resulting coefficients are averaged to produce mean fields.

The two climatologies have been shown to be very similar when compared at comparable resolutions, i.e., when the GDEM fields are filtered to the resolution of the LC fields. Derived dynamic height differences between the climatologies are largest in intense current regions such as the Gulf Stream and Kuroshio but are otherwise relatively small (less than 5 cm) over much of the three ocean basins analyzed. In those small-difference areas (e.g., in the middle of the Sargasso Sea) there were few significant differences between the $\frac{1}{2}°$ GDEM and the 1° GDEM. However, in regions such as the Gulf Stream the unsmoothed $\frac{1}{2}°$ GDEM climatology clearly provides a better description than the 1° GDEM or LC. Grids of 1°–2° are adequate for describing much of the Atlantic, Pacific, and Indian oceans outside of regions of large current shear, but finer grids are needed to delineate major currents.

For the Atlantic and Pacific oceans, weak seasonality was indicated from LC. Small seasonal anomalies in dynamic height fields were ±10 cm and were less than ±5 cm for large areas. In contrast, a stronger seasonality is found from GDEM for the Atlantic and Pacific oceans. Its anomalies are almost twice as large, ranging from −15 cm to 20 cm. However, GDEM and LC anomalies are comparable for most of the Indian Ocean, ranging from 5 cm to 15 cm in magnitude, except for the region between 30°S and 40°S. There LC anomalies surpass 15 cm, while GDEM anomalies are 5–10 cm. LC anomaly magnitudes were smaller than GDEM anomaly magnitudes for the Atlantic and Pacific oceans but larger than GDEM anomaly magnitudes for the Indian Ocean. The larger LC anomalies for the Indian Ocean could be attributed to the highly contrasting monsoon seasons. A more likely explanation, however, is that lower data densities used in LC formulation produced less representative data fields than in GDEM formulation. It is concluded that there is less seasonal signal in LC dynamic heights than in GDEM dynamic heights for the Atlantic and Pacific oceans. LC dynamic heights appear less reliable than GDEM dynamic heights for the Indian Ocean between 30°S and 40°S.

The larger seasonal variability in GDEM when compared to that of LC is also seen in annual rms variability maps (Figure 18), which were computed for GDEM and LC dynamic height fields according to

$$\text{rms} = \sqrt{\frac{1}{4}\sum_{i=1}^{4}(H_i - \bar{H})^2} \qquad (11)$$

where H_i is the seasonal value and $\bar{H}$ is the annual mean value computed from the four seasonal values. Variability was generally greater in magnitude for smoothed GDEM than for LC for both the Atlantic and the Pacific, but both produced similar results for the Indian Ocean. In particular, LC variability for the Gulf Stream was far too low, a result probably due to the inherent smoothing.

Unsmoothed GDEM rms variability patterns (Figure 19*b*) for the Gulf Stream compare qualitatively very well with the surface variability patterns computed from GEOSAT altimetry data (Figure 19*a*) [*Mitchell*, 1990]. The major highs in the height fields, west of the New England seamounts near 69°W and east of the seamounts between 50°W and 60°W, are seen in both data sets. This agreement is remarkable, since analysis of the 1-year GEOSAT record (1987) can only resolve periods between 34 days and 1 year, while the GDEM result is an average of 66 years of observations, effectively removing interannual variability. The quantitatively higher rms height (by about 25%) in the GEOSAT result is likely caused by contamination from the interannual signal. Peak values are near 30 cm for GDEM rms heights and near 40 cm for altimetric rms heights.

Both GDEM and LC density fields are used extensively at the Naval Ocean Research and Development Activity (NORDA) and at Fleet Numerical Oceanographic Center for initialization of numerical models. Only LC provides full coverage for global ocean models. However, unsmoothed GDEM (where available) provides better delineation of current shear and seasonality for regional models with grid spacings of $\frac{1}{2}°$ or less. Additionally, all depth levels are available in GDEM, inherent from the storing of profiles as coefficients. One of the principal advantages of GDEM over LC, particularly in short-term forecasts of about a week, is that GDEM was designed for continuous interpolation in time. This capability has proven to be valuable at NORDA in Gulf Stream forecasts. For the oceanographic community as a whole, GDEM has not been as greatly utilized as LC, since it has not been as readily available, a situation that may be

remedied in the near future. Presently, GDEM is available to investigators working on U.S. Navy contracts. However, when a worldwide climatology is required, LC may remain as the only one available. The plan is to blend it with GDEM in the future to fill in data void regions within GDEM, making GDEM a global climatology.

More climatology examination is obviously needed. For example, vertical profiles should be examined in detail and compared with in situ data. Dynamic GDEMs should also be evaluated, as they are an important new form of climatology. These are future projects in the NORDA plans.

Acknowledgments. We would like to thank Harley E. Hurlburt of NORDA for his advice and encouragement. Thanks are extended to the developers of GDEM, Thomas M. Davis and Kenneth A. Countryman of the Naval Oceanographic Office, for their assistance. Thanks are also extended to Zachariah R. Hallock, Kim D. Saunders, Michael R. Carnes, and Albert W. Green of NORDA and Gary Ransford of Sverdrup Technology, Inc., for their helpful suggestions and review. This research was supported by the Office of Naval Research under program element 62435N and NORDA project 3584 803 as part of the Global and Regional Modeling Project under the Naval Ocean Modeling Program. This document, NORDA contribution JA 331:057:89, has been reviewed and is approved for public release.

REFERENCES

Bauer, R. A., Functional description Master Oceanographic Observation Data Set (MOODS), Compass Systems, Inc., San Diego, Calif., 1985.

Boston, M. A., Program performance specification for the sound speed profile module, *Tech. Note TESS 87-09*, 31 pp., U.S. Nav. Oceanogr. Office, Washington, D. C., 1987.

Briggs, I. C., Machine contouring using minimum curvature, *Geophysics*, *39*, 39–48, 1984.

Cressman, G. P., An operational objective analysis scheme, *Mon. Weather Rev.*, *87*, 329–340, 1959.

Davis, T. M., K. A. Countryman, and M. J. Carron, Tailored acoustic products utilizing the NAVOCEANO GDEM (a generalized digital environmental model), in *Proceedings, 36th Naval Symposium on Underwater Acoustics*, Naval Ocean Systems Center, San Diego, Calif., 1986.

Farebrother, R. W., *Linear Least Squares Computations*, pp. 223–227, Marcel Dekker, New York, 1988.

Fuglister, F. C., *Atlantic Ocean Atlas*, 209 pp., Woods Hole Oceanographic Institute, Woods Hole, Mass., 1960.

Gonzalez-Casanova, P., and R. Alvarez, Splines in geophysics, *Geophysics*, *50*, 2831–2848, 1985.

Kao, T. W., The Gulf Stream and its frontal structure: A quantitative representation, *J. Phys. Oceanogr.*, *17*, 123–133, 1987.

Levitus, S., Climatological atlas of the world ocean, *NOAA Prof. Pap.*, *13*, 173 pp., 1982.

Martin, M. A., Frequency domain applications in data processing, *Doc. 57SD340*, General Electric, Philadelphia, Pa., May 1957.

Mitchell, J. L., J. M. Dastugue, W. J. Teague, and Z. R. Hallock, The estimation of geoid profiles in the NW Atlantic from simultaneous satellite altimetry and AXBT sections, *J. Geophys. Res.*, in press, 1990.

Robinson, M. K., Atlas of the North Pacific monthly mean temperatures and mean salinities of the surface layer, *Ref. Publ. 2*, 173 pp., U.S. Nav. Oceanogr. Office, Washington, D. C., 1976.

Robinson, M. K., R. A. Bauer, E. H. Schroeder, Atlas of North Atlantic–Indian Ocean monthly mean temperatures and salinities of the surface layer, *Ref. Publ. 18*, 213 pp., U.S. Naval Oceanogr. Office, Washington, D. C., 1979.

Oppenheim, A. V., and R. W. Schafer, *Digital Signal Processing*, pp. 211–212, Prentice-Hall, Englewood Cliffs, N. J., 1975.

Schuman, F. G., Numerical methods in weather prediction, II, Smoothing and filtering, *Mon. Weather Rev.*, *85*, 357–361, 1957.

Stommel, H., and M. Fieux, *Oceanographic Atlases, A Guide to Their Geographic Coverage and Contents*, 97 pp., Woods Hole Press, Woods Hole, Mass., 1978.

Swain, C. J., A FORTRAN IV Program for interpolating irregularly spaced data using the difference equations for minimum curvature, *Comput. Geosci.*, *1*, 231–240, 1976.

Teague, W. J., E. J. Molinelli, and M. J. Carron, A new system for management of the "Master Oceanographic Observation Data Set" (MOODS), *Eos Trans. AGU*, *68*, 553, 558–559, 1987.

Worthington, L. V., and W. R. Wright, *North Atlantic Ocean Atlas*, 24 pp., Woods Hole Oceanographic Institute, Woods Hole, Mass., 1970.

Wüst, G., and A. Defant, Atlas zur Schichtung and Zirkulation des Atlantischen Ozeans, Schnitte und Karten von Temperatur, Salzegehalt, und Dichte, in *Deutsche Atlantische Expedition auf dem Forschungs- und Vermessungsschiff Meteor, 1925–1927, Wissenschaftliche Ergebnisse*, vol. 6, Walter de Gruyter, Berlin, 1936.

Wylie, C. R., Jr., *Advanced Engineering Mathematics*, pp. 156–160, McGraw-Hill, New York, 1975.

Wyrtki, K., *Oceanographic Atlas of the Indian Ocean Expedition*, 531 pp., National Science Foundation, Washington, D. C., 1971.

M. J. Carron, Naval Oceanographic Office, Stennis Space Center, MS 39529.

P. J. Hogan, Sverdrup Technology, Inc., Stennis Space Center, MS 39529.

W. J. Teague, NORDA, Building 1105, Room 124, Stennis Space Center, MS 39529.

(Received August 17, 1989;
revised October 23, 1989;
accepted November 20, 1989.)